Journal of Solid State Chemistry **145,** 694–704 (1999)
Article ID jssc.1999.8281, available online at http://www.idealibrary.com on IDEAL®

A Layered Solution Crystal Growth Technique and the Crystal Structure of $(C_6H_5C_2H_4NH_3)_2PbCl_4$

D. B. Mitzi

IBM T. J. Watson Research Center, P. O. Box 218, Yorktown Heights, New York 10598

Received January 20, 1999; in revised form March 9, 1999; accepted March 13, 1999

Single crystals of the organic–inorganic perovskite $(C_6H_5C_2H_4NH_3)_2PbCl_4$ have been grown at room temperature using a layered solution approach. The bottom solution layer, contained within a long straight tube, consists of $PbCl_2$ dissolved in concentrated aqueous HCl. A less dense layer of methanol is carefully placed on top of the HCl/$PbCl_2$ solution using a syringe. Finally, a stoichiometric quantity of $C_6H_5C_2H_4NH_2$ (relative to the $PbCl_2$) is added to the top of the column. As the layers slowly diffuse together, well-formed crystals of $(C_6H_5C_2H_4NH_3)_2PbCl_4$ appear near the interface between the HCl/$PbCl_2$ and $C_6H_5C_2H_4NH_2$ solutions. The thick, plate-like crystals are well suited for X-ray crystallography studies. Room temperature intensity data were refined using a triclinic ($P\bar{1}$) cell ($a = 11.1463(3)$ Å, $b = 11.2181(3)$ Å, $c = 17.6966(5)$ Å, $\alpha = 99.173(1)^\circ$, $\beta = 104.634(1)^\circ$, $\gamma = 89.999(1)^\circ$, $V = 2111.8(1)$ Å^3, $Z = 4$, $R_f/R_w = 0.031/0.044$). The organic–inorganic layered perovskite structure features well-ordered sheets of corner-sharing distorted $PbCl_6$ octahedra separated by bilayers of phenethylammonium cations. Tilting and rotation of the $PbCl_6$ octahedra within the perovskite sheets, coupled with organic cation ordering, leads to the unusual in-sheet $2a_p \times 2a_p$ superstructure, where a_p is the lattice constant for the ideal cubic perovskite. © 1999 Academic Press

INTRODUCTION

Substantial attention has recently been focused on the layered organic–inorganic perovskites $(C_6H_5C_2H_4NH_3)_2PbX_4$ (X = Cl, Br, and I) as a result of the strong photoluminescence (1–5), electroluminescence (6, 7), nonlinear optical properties (8), and tunable polariton absorption (9) observed in these systems. In fact, these and other related organic–inorganic perovskites (10) can be considered natural multiple quantum well structures, with the metal halide sheets acting as wells and the much wider bandgap organic layers serving as barriers. The unusual optical properties in these systems arise from the presence of exciton states, with very large binding energy, within the metal halide sheets. In $(C_6H_5C_2H_4NH_3)_2PbI_4$, for example, the 220($\pm$30) meV exciton binding energy (1) is substantially larger than k_BT at room temperature ($\approx$25 meV), enabling the effects of the excitons to be observed at room temperature.

Detailed structural analysis of the systems $(C_6H_5C_2H_4NH_3)_2PbX_4$ (X = Cl, Br, and I) has so far been limited. The low temperature ($T \approx 200$ K) structure of $(C_6H_5C_2H_4NH_3)_2PbI_4$ has been reported (8) in the monoclinic space group $C2/m$, with the lattice constants $a = 32.508(5)$ Å, $b = 6.131(1)$ Å, $c = 6.185(1)$ Å, and $\beta = 93.80(1)^\circ$. However, in the proposed structural model, both the bridging iodide ions and the phenethylammonium cations are disordered across mirror planes. Since the organic cations are poorly located, issues of phenethylammonium cation conformation and bonding interactions are difficult to address. Powder diffraction studies on the series $(C_6H_5C_2H_4NH_3)_2PbX_4$ (X = Cl, Br, and I) suggest (11) that the structures are isomorphous, with the a and b lattice constants expanding and the long c axis (perpendicular to the perovskite sheets) contracting as a function of increasing anion size. Similar data from mixed anion systems are more difficult to interpret based on a model in which the compounds are considered isostructural. While the $(C_6H_5C_2H_4NH_3)_2PbCl_xBr_{4-x}$ system yields a smooth progression in the c-axis dimension as a function of x, analogous data for the $(C_6H_5C_2H_4NH_3)_2PbBr_xI_{4-x}$ system demonstrate a sharp break in the c-axis lattice parameter (suggesting a structural transition) at approximately $x = 1$ (5). Furthermore, ^{1}H NMR measurements (11) indicate that there are two types of NH_3 sites in the X = Cl and Br structures, but only one for X = I. Clearly single crystal diffraction studies are needed to clarify the structural issues within this family.

One difficulty in the crystallographic study of the organic–inorganic perovskites is the growth of suitable single crystals. Generally, as a result of the highly anisotropic nature of the layered perovskite structures, crystals tend to grow as thin flakes, leading to problems with weak diffraction and crystal distortion during the mounting process. In this contribution, we report a layered solution crystal growth technique that yields thick, well-formed crystals of $(C_6H_5C_2H_4NH_3)_2PbCl_4$ (as well as other related systems),

0022-4596/99 $30.00

enabling an examination of the detailed crystal structure of this compound.

EXPERIMENTAL

1. Crystal Growth

Crystals of $(C_6H_5C_2H_4NH_3)_2PbCl_4$ were grown at room temperature within a long, straight, glass tube (Fig. 1) by first dissolving 1.0 mmol (0.278 g) of freshly sublimed $PbCl_2$ (Aldrich; 99.999%) in 7.5 ml concentrated (37 wt %) aqueous HCl (Aldrich; 99.999%). In order to maintain a nominally inert atmosphere during the crystal growth, the $PbCl_2$ was weighed and added to the tube in an argon-filled glove box, with oxygen and water levels maintained below 1 ppm.

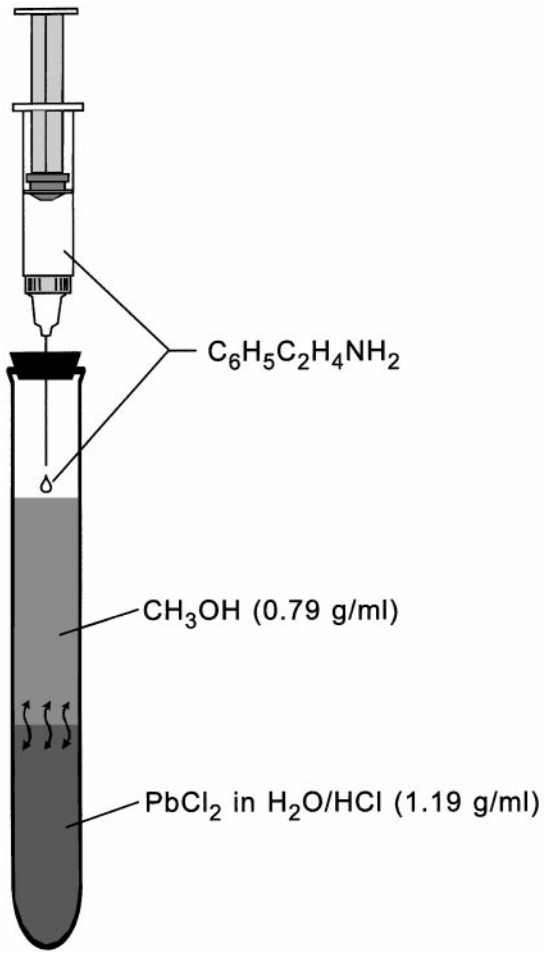

FIG. 1. Schematic diagram of the layered solution crystal growth setup, with the densities of the pure solvents in each layer shown in parentheses. The most dense layer, consisting of $PbCl_2$ in a concentrated aqueous HCl solution, is placed on the bottom of a long narrow glass tube. A less dense layer of methanol is placed on top of the $PbCl_2$ solution and a few drops (stoichiometric amount) of phenethylamine are added to the top of the column. As the components diffuse together crystals form, primarily at the interface between the two solutions.

The tube was covered with a septum before removing from the glove box and the HCl was added with a syringe.

A second layer within the crystal growth tube (Fig. 1) was created by gently syringing 15 ml of methanol (Aldrich; anhydrous, 99.8%) on top of the HCl/$PbCl_2$ solution. Note that because of the density difference between the HCl and methanol solutions (nominally 1.190 vs 0.791 g/ml for the pure solvents), a relatively sharp interface can be created between the solvent layers. Upon adding the methanol, a small amount of precipitate (presumably $PbCl_2$) formed at the interface, but disappeared during the course of the crystal growth. On top of the column, a stoichiometric amount (2 mmol or approximately 0.25 ml) of phenethylamine was carefully added with a syringe. The phenethylamine rapidly dispersed in the methanol but, because of the sharp interface with the HCl solution, the formation of the final $(C_6H_5C_2H_4NH_3)_2PbCl_4$ product was very slow. Over several weeks, crystals were observed growing at the interface between the solutions (which slowly diffused together). The crystals were isolated after approximately one year by removing the solvent with a syringe and drying the crystals under vacuum at room temperature. The colorless $(C_6H_5C_2H_4NH_3)_2PbCl_4$ crystals ranged in habit from small block-like crystals useful for X-ray diffraction studies to larger plate-like crystals (dimensions > 4 mm). The crystals were subsequently stored in an argon-filled glove box.

2. X-Ray Diffraction

A colorless single crystal of $(C_6H_5C_2H_4NH_3)_2PbCl_4$, with approximate dimensions $0.09\text{ mm} \times 0.18\text{ mm} \times 0.27\text{ mm}$, was selected under a microscope and attached to the end of a quartz fiber with 5 minute epoxy. A full sphere of data was collected at room temperature on a Bruker SMART CCD diffractometer, equipped with a normal focus 2.4 kW sealed tube X-ray source (Mo$K\alpha$ radiation, $\lambda = 0.71073$ Å). The crystal was maintained in a gentle stream of ambient temperature dry nitrogen gas during the measurement. Intensity data were collected with a detector distance of approximately 5.0 cm, in 3600 frames with increasing ω, and an exposure time of 60 sec per frame. The increment in ω between each frame was 0.2°. Instrument and crystal stability were monitored and the maximum variations in I were $< 0.7\%$.

The initial triclinic unit cell was selected based on an indexing of 730 reflections. Note that a triclinic cell is somewhat unusual for single layer organic–inorganic perovskite structures (e.g., see Table II in Ref. (10)). Generally, higher symmetry (monoclinic or orthorhombic) structures are observed. In fact, artificially doubling the c-axis dimension of the observed triclinic cell leads to a cell which can then be transformed to an A-centered nominally monoclinic cell with $a = 11.1463(3)$ Å, $b = 11.2181(3)$ Å,

$c = 67.698(1)$ Å, $\alpha = 90.056(1)^\circ$, $\beta = 93.734(1)^\circ$, and $\gamma = 90.001(1)^\circ$. Attempts to solve the structure in this larger monoclinic cell did not yield a satisfactory structure or refinement. The substantial absence of superstructure peaks in the CCD frames and the successful structural refinement in the smaller unit cell ultimately led to the adoption of the triclinic cell for the structural description. The final unit cell parameters and crystal orientation matrix were obtained by a least-squares fit of 8192 reflections. An empirical absorption correction, based on equivalent reflections, was applied to the intensity data (12).

The structure was solved and refined using the NRCVAX 386 PC version program (13). First, the Pb and Cl atoms were located using direct methods. The N and C atoms were then located using a single Fourier difference map. All nonhydrogen atoms were refined anisotropically. While the H atoms could be located within the final Fourier difference map, they were not included in the refinement. The minimum and maximum peaks in the final difference Fourier map corresponded to -1.86 and 2.97 e/Å^3, with the first five residual peaks all appearing within 0.75 Å of either Pb(1) or Pb(2). No additional symmetry was detected using the MISSYM program (14). The crystallographic results are summarized in Table 1. The atom labeling, connectivity, and thermal ellipsoids are depicted in Fig. 2, with the atomic coordinates, heavy atom anisotropic displacement parameters, and bond distances and angles listed in Tables 2, 3, and 4, respectively.

TABLE 1
Data Collection and Structure Refinement Parameters

Formula	$(C_6H_5C_2H_4NH_3)_2PbCl_4$
Formula weight	593.4
Space group	$P\bar{1}$ (No. 2)
a, Å	11.1463(3)
b, Å	11.2181(3)
c, Å	17.6966(5)
α, °	99.173(1)
β, °	104.634(1)
γ, °	89.999(1)
V, Å^3	2111.8(1)
Z	4
ρ_{calcd}, g/cm^3	1.866
Absorption coefficient (μ), mm^{-1}	8.51
Maximum 2θ, °	55
No. of reflections collected	24415
No. of unique reflections	9661
No. of reflections used in refinement	8298 ($I > 2\sigma(I)$)
R_{int}	0.013
No. of variables	416
Secondary extinction coefficient (μm)	0.500
R_f^a	0.031
R_w^b	0.044
Goodness of fit (GoF)^c	1.91

$^aR_f = \sum(F_o - F_c)/\sum(F_o)$.
$^bR_w = \{\sum w(F_o - F_c)^2/\sum(wF_o^2)\}^{1/2}$.
$^c\text{GoF} = \{\sum w(F_o - F_c)^2/(n-m)\}^{1/2}$; where n is the number of reflections and m is the number of refinement parameters.

RESULTS AND DISCUSSION

1. Layered Solution Crystal Growth

One trend in the field of organic–inorganic hybrids involves the replacement of relatively simple organic cation components with more complex and functional organic cations (10). The impetus for this substitution is the desire to create multifunctional hybrids where both the inorganic and organic components contribute selected properties or functionality to the hybrid. A simple example of this is the replacement, within the layered perovskite structure, of an aliphatic with an aromatic ammonium cation, with the goal of altering the dielectric constant of the organic layer and thereby tailoring the properties of the excitons within the inorganic framework (1). A more recent example involves the incorporation of dye molecules within the layered perovskite framework (10). As more complex organic–inorganic systems are considered, alternative crystal growth techniques are required to overcome difficulties with poor crystal quality for crystals grown (or the inability to grow crystals) using standards solution processes.

A number of solution techniques have been demonstrated (10, 15) for growing crystals of simple organic–inorganic perovskites. These techniques generally involve the slow cooling or evaporation of a homogeneous saturated solution. Well-formed crystals of $(C_4H_9NH_3)_2MI_4$ (M = Ge, Sn, and Pb), for example, can be grown from slowly cooled, aqueous hydriodic acid solutions containing a stoichiometric mixture of $C_4H_9NH_2 \cdot HI$ and MI_2 (16). Using the same solution technique for the $(C_6H_5C_2H_4NH_3)_2PbX_4$ (X = Cl, Br, and I) compounds, however, generally yields very thin flakes or sheet-like crystals which are difficult to handle for many studies (e.g., crystallography). Marginally satisfactory crystals of the phenethylammonium-based perovskites have also been grown using a mixed tetrahydrofuran (THF)/ether solution (8).

In contrast to the slow cooling or evaporation techniques, which generally rely on homogeneous solutions, single crystals of the long-chain alkylammonium lead(II) iodides, $(C_nH_{2n+1}NH_3)_2PbI_4$ ($n = 8, 9, 10, 12$), and the inorganic perovskites, $ASnX_3$ ($A = Rb^+$ or Cs^+ an $X = Cl^-$, Br^-, or I^-), have been grown using a silica-gel process (17, 18). In this case, a gel barrier controls diffusion among the components of the desired product during crystal growth (or, alternatively, some of the components are incorporated in the gel to begin with). As the soluble components diffuse together through the gel, crystals of the less soluble product form within the gel. While well-formed crystals can be achieved, gel components generally contaminate the product (19).

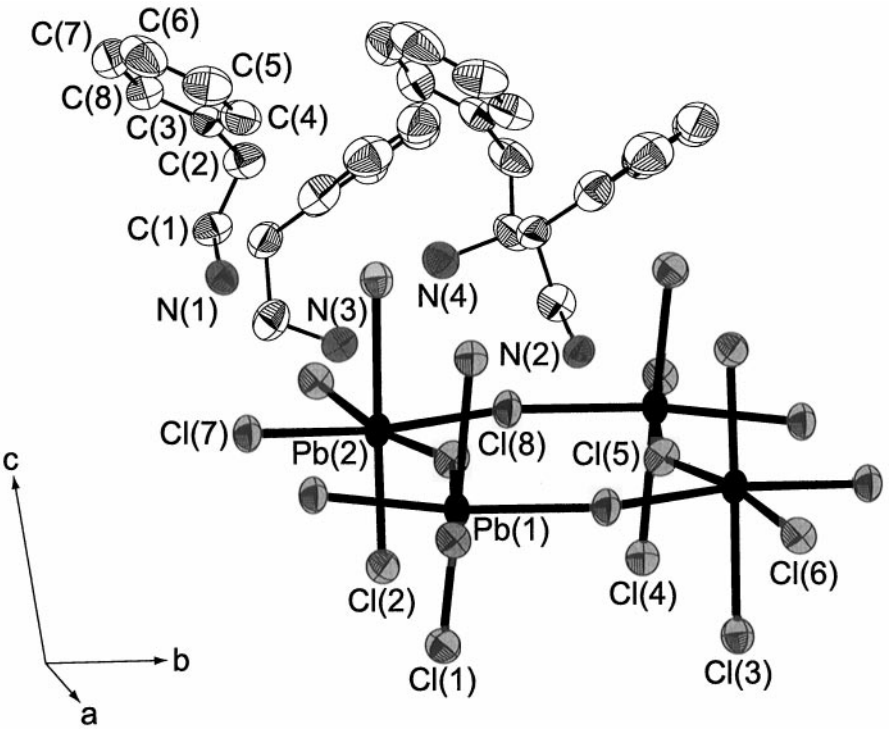

FIG. 2. ORTEP plot (50% probability ellipsoids) showing the atom labeling and thermal ellipsoids for the $(C_6H_5C_2H_4NH_3)_2PbCl_4$ structure. For clarity, the carbon atom labels for only one of the four independent phenethylammonium cations are shown.

As shown in this contribution, rather than using a gel to prevent quick mixing of the organic and inorganic components, the two species can be dissolved in separate, nominally miscible solvents that have substantially different density. The two solutions are carefully placed on top of each other in a long narrow tube, with the barrier to diffusion effectively becoming the density difference and the degree of miscibility of the two solvents, rather than the presence of a gel. Consequently, the contamination from the gel can be fully avoided. Some of the parameters that are important in this process are the concentrations of the solutes in the different layers of the solution, the degree of solubility of the starting materials and the final product in each of the solvents, the densities and degree of miscibility of the two solvents (or mixtures of solvents), and the solution temperature during crystal growth.

In the layered solution growth of $(C_6H_5C_2H_4NH_3)_2PbCl_4$ crystals, for example, the solvents are concentrated aqueous hydrochloric acid ($d = 1.19$ g/ml) for the inorganic component and methanol ($d = 0.79$ g/ml) for the organic component. The two solvents are substantially miscible, but the density difference between the two provides an effective impediment to mixing. Phenethylamine is highly soluble in methanol and lead(II) chloride is soluble in the acid solution (although it is quite slow to go into solution). However, the perovskite product is less soluble in the solvent mixture than either of the two starting component chloride salts, thereby providing an effective system for growing crystals as the two solutions diffuse together. Since both the organic or inorganic components of the structure are thermally stable, the crystal growth can be accomplished at room temperature without cooling.

The layered solution technique is expected to be especially useful for materials which exhibit an unsuitable crystal habit when grown using other techniques (as for $(C_6H_5C_2H_4NH_3)_2PbCl_4$) or in which the organic and inorganic components have incompatible solubility requirements. Systems in which one or more components require cooling to prevent polymerization or decomposition are also particularly appropriate since the low temperatures generally would render slow cooling or evaporation processes impractical. In addition to the $(C_6H_5C_2H_4NH_3)_2PbX_4$ ($X = Cl$) crystals, which form the focus of this study, well-formed $X = Br$ crystals have also been grown using the same layered solution process. During the $X = Br$ crystal growth, a substantial quantity of crystals could be observed after only two weeks and therefore crystals were isolated at this point (rather than after 1 year as for the $X = Cl$ experiment). During the process of removing the solvents from the crystal growth tube, a substantial amount of

TABLE 2
Positional and Thermal Parameter Data for $(C_6H_5C_2H_4NH_3)_2PbCl_4$

Atom	x	y	z	B_{iso} (Å^2)
Pb(1)	0.75448(1)	0.24327(1)	0.01056(1)	2.53(1)
Pb(2)	0.25455(1)	0.26211(2)	0.01051(1)	2.51(1)
Cl(1)	0.8086(2)	0.3007(1)	0.1730(1)	3.92(6)
Cl(2)	0.3104(2)	0.2853(1)	0.1731(1)	3.88(6)
Cl(3)	0.1931(1)	0.2315(1)	− 0.1683(1)	3.60(6)
Cl(4)	0.6942(1)	0.1842(1)	− 0.1686(1)	3.57(6)
Cl(5)	0.0017(1)	0.1890(1)	− 0.0010(1)	3.50(6)
Cl(6)	0.5015(1)	0.3105(1)	− 0.0013(1)	3.50(6)
Cl(7)	0.8103(1)	0.4880(1)	0.0008(1)	3.75(6)
Cl(8)	0.6900(1)	− 0.0122(1)	− 0.0002(1)	3.79(6)
N(1)	0.6353(4)	0.5254(4)	0.1441(3)	3.6(2)
C(1)	0.5241(5)	0.5464(6)	0.1792(4)	4.0(3)
C(2)	0.5642(6)	0.6160(6)	0.2614(4)	4.6(3)
C(3)	0.6479(6)	0.5461(5)	0.3214(4)	3.8(3)
C(4)	0.7749(8)	0.5811(7)	0.3477(4)	4.9(3)
C(5)	0.8564(7)	0.5147(8)	0.3988(5)	6.0(4)
C(6)	0.8088(9)	0.4186(8)	0.4248(5)	7.1(5)
C(7)	0.6788(9)	0.3867(7)	0.3999(5)	6.2(4)
C(8)	0.5996(7)	0.4519(6)	0.3468(4)	4.7(3)
N(2)	0.8659(4)	− 0.0461(4)	− 0.1424(3)	3.4(2)
C(9)	0.9771(5)	− 0.0447(6)	− 0.1779(4)	4.2(3)
C(10)	0.9345(6)	− 0.0165(6)	− 0.2649(4)	4.4(3)
C(11)	0.8538(6)	− 0.1174(5)	− 0.3210(4)	3.7(3)
C(12)	0.7296(8)	− 0.0979(7)	− 0.3466(5)	5.1(4)
C(13)	0.6533(8)	− 0.1923(9)	− 0.4008(5)	6.6(4)
C(14)	0.7000(8)	− 0.2986(8)	− 0.4259(5)	6.0(4)
C(15)	0.8256(9)	− 0.3141(7)	− 0.3977(5)	5.9(4)
C(16)	0.9029(6)	− 0.2237(6)	− 0.3470(4)	4.6(3)
N(3)	0.9369(4)	0.3687(4)	− 0.1436(3)	3.9(2)
C(17)	0.9203(6)	0.4868(6)	− 0.1759(4)	4.8(3)
C(18)	0.9400(7)	0.4693(6)	− 0.2619(4)	5.1(3)
C(19)	0.8535(6)	0.3761(6)	− 0.3211(4)	4.0(3)
C(20)	0.7286(8)	0.3998(8)	− 0.3497(5)	5.1(4)
C(21)	0.6512(7)	0.3150(9)	− 0.4051(5)	6.4(5)
C(22)	0.6915(8)	0.2058(8)	− 0.4340(5)	6.4(4)
C(23)	0.8160(9)	0.1822(7)	− 0.4039(5)	6.4(5)
C(24)	0.8976(7)	0.2678(6)	− 0.3500(4)	4.9(4)
N(4)	0.4384(4)	0.0608(4)	− 0.1447(3)	4.3(2)
C(25)	0.5806(6)	0.0751(6)	0.1777(4)	4.8(3)
C(26)	0.5585(7)	0.0988(6)	0.2571(4)	5.4(3)
C(27)	0.6459(6)	0.0343(5)	0.3219(4)	4.2(3)
C(28)	0.5993(6)	− 0.0571(6)	0.3522(4)	5.0(3)
C(29)	0.6761(9)	− 0.1154(7)	0.4084(5)	6.2(4)
C(30)	0.801(1)	− 0.0831(8)	0.4305(5)	7.7(5)
C(31)	0.8506(7)	0.0099(9)	0.3986(5)	6.6(5)
C(32)	0.7696(8)	0.0705(8)	0.3467(5)	5.2(4)

further crystallization occurred as the two solution layers were disturbed and therefore mixed. This observation highlights the fact that the diffusion between the layers is slow and may take substantially more than two weeks to complete. In addition to the growth of the phenethylammonium lead(II) halides, a preliminary description of the layered solution growth technique has also recently appeared (10, 20) for the corresponding thiophene-3-ethylammonium lead(II) halide systems. In this case, cooling of the crystal growth solution is important to prevent degradation–polymerization of the organic cation. As for the crystal growth of $(C_6H_5C_2H_4NH_3)_2PbCl_4$, well-formed, relatively thick, plate-like crystals were achieved using the layered solution technique.

2. *Crystal Structure of $(C_6H_5C_2H_4NH_3)_2PbCl_4$*

The basic building block of the $(C_6H_5C_2H_4NH_3)_2PbCl_4$ structure, as shown in Fig. 3, consists of a well-ordered layer of corner-sharing $PbCl_6$ octahedra (i.e., a perovskite sheet), with a layer of phenethylammonium cations capping the inorganic sheet on both sides. The organic cations hydrogen bond to halogens in the perovskite layer through the ammonium group on each molecule. The full three-dimensional structure is then created by stacking the neutral organic-sheathed $(C_6H_5C_2H_4NH_3)_2PbCl_4$ units along the c axis. Weak (e.g., van der Waals) interactions between the phenyl groups of successive $(C_6H_5C_2H_4NH_3)_2PbCl_4$ layers hold the structure together, with no interleaving among the phenethylammonium cations from adjacent layers.

The perovskite sheets consist of two independent Pb atoms. Each has a very similar distorted octahedral chloride coordination (Fig. 2; Table 4), with Pb–Cl bond lengths ranging from 2.752(2) to 3.033(2) Å and Cl–Pb–Cl bond angles ranging from 83.11(4)° to 97.26(4)° and 171.01(4)° to 179.08(4)° (for angles which would be 90° and 180°, respectively, for a perfect octahedral coordination). The average Pb–Cl bond length for the two $PbCl_6$ octahedra is 2.886 Å. Note that the bridging Pb(1)–Cl–Pb(2) bond angles are

TABLE 3
Selected Anisotropic Displacement Parameters, U_{ij} (×100)[a], for $(C_6H_5C_2H_4NH_3)_2PbCl_4$

Atom	U_{11}	U_{22}	U_{33}	U_{12}	U_{13}	U_{23}
Pb(1)	2.56(1)	2.49(1)	4.65(1)	0.129(6)	1.080(8)	0.561(7)
Pb(2)	2.57(1)	2.61(1)	4.55(1)	0.154(6)	1.068(8)	0.924(7)
Cl(1)	5.34(8)	4.77(8)	4.53(9)	0.77(6)	0.75(7)	0.86(6)
Cl(2)	5.40(9)	4.73(8)	4.32(8)	− 0.53(6)	0.74(6)	0.63(6)
Cl(3)	4.12(7)	4.34(7)	4.98(9)	− 0.05(5)	0.77(6)	0.69(6)
Cl(4)	4.09(7)	4.49(7)	4.77(8)	0.16(5)	0.69(6)	0.86(6)
Cl(5)	2.85(6)	5.27(8)	5.31(9)	0.32(5)	0.97(6)	1.43(6)
Cl(6)	2.93(6)	4.99(8)	5.23(9)	0.03(5)	1.03(6)	0.39(6)
Cl(7)	5.85(9)	3.01(6)	5.66(9)	0.25(5)	1.90(7)	0.84(5)
Cl(8)	5.86(9)	3.12(6)	5.71(9)	0.30(5)	1.85(7)	1.04(6)

[a] The anisotropic displacement factor expression is: $\exp[-2\pi^2(U_{11}h^2a^{*2} + U_{22}k^2b^{*2} + U_{33}l^2c^{*2} + 2U_{12}hka^*b^* + 2U_{13}hla^*c^* + 2U_{23}klb^*c^*)]$.

TABLE 4
Selected Bond Distances (Å) and Angles (°) in $(C_6H_5C_2H_4NH_3)_2PbCl_4$

Pb(1)–Cl(1)	2.752(2)	Cl(6)–Pb(1)–Cl(8)	92.34(4)
Pb(1)–Cl(4)	3.033(2)	Cl(7)–Pb(1)–Cl(8)	173.11(4)
Pb(1)–Cl(5)	2.873(1)	Cl(2)–Pb(2)–Cl(3)	178.91(4)
Pb(1)–Cl(6)	2.883(1)	Cl(2)–Pb(2)–Cl(5)	90.64(4)
Pb(1)–Cl(7)	2.857(1)	Cl(2)–Pb(2)–Cl(6)[a]	96.95(4)
Pb(1)–Cl(8)	2.919(1)	Cl(2)–Pb(2)–Cl(7)[b]	97.26(4)
Pb(2)–Cl(2)	2.754(2)	Cl(2)–Pb(2)–Cl(8)[c]	89.98(4)
Pb(2)–Cl(3)	3.025(2)	Cl(3)–Pb(2)–Cl(5)	89.05(4)
Pb(2)–Cl(5)	2.883(1)	Cl(3)–Pb(2)–Cl(6)[a]	83.28(4)
Pb(2)–Cl(6)[a]	2.872(1)	Cl(3)–Pb(2)–Cl(7)[b]	83.80(4)
Pb(2)–Cl(7)[b]	2.920(1)	Cl(3)–Pb(2)–Cl(8)[c]	88.96(4)
Pb(2)–Cl(8)[c]	2.858(1)	Cl(5)–Pb(2)–Cl(6)[a]	171.05(4)
N(1)–C(1)	1.523(7)	Cl(5)–Pb(2)–Cl(7)[b]	92.29(4)
C(1)–C(2)	1.50(1)	Cl(5)–Pb(2)–Cl(8)[c]	87.34(4)
C(2)–C(3)	1.54(1)	Cl(6)[a]–Pb(2)–Cl(7)[b]	91.45(4)
C(3)–C(4)	1.41(1)	Cl(6)[a]–Pb(2)–Cl(8)[c]	87.92(4)
C(4)–C(5)	1.41(1)	Cl(7)[b]–Pb(2)–Cl(8)[c]	172.76(4)
C(5)–C(6)	1.39(1)	Pb(1)–Cl(5)–Pb(2)	151.45(5)
C(6)–C(7)	1.43(1)	Pb(1)–Cl(6)–Pb(2)[d]	151.37(5)
C(7)–C(8)	1.41(1)	Pb(1)–Cl(7)–Pb(2)[b]	153.21(5)
C(8)–C(3)	1.372(9)	Pb(1)–Cl(8)–Pb(2)[c]	153.28(5)
N(2)–C(9)	1.525(7)	N(1)–C(1)–C(2)	110.2(5)
C(9)–C(10)	1.58(1)	C(1)–C(2)–C(3)	114.0(5)
C(10)–C(11)	1.51(1)	C(2)–C(3)–C(4)	117.7(6)
C(11)–C(12)	1.37(1)	C(2)–C(3)–C(8)	120.6(6)
C(12)–C(13)	1.42(1)	C(3)–C(4)–C(5)	119.6(7)
C(13)–C(14)	1.36(1)	C(4)–C(5)–C(6)	119.3(7)
C(14)–C(15)	1.38(1)	C(5)–C(6)–C(7)	120.5(7)
C(15)–C(16)	1.38(1)	C(6)–C(7)–C(8)	119.2(7)
C(16)–C(11)	1.37(1)	C(7)–C(8)–C(3)	119.7(7)
N(3)–C(17)	1.518(7)	C(8)–C(3)–C(4)	121.6(6)
C(17)–C(18)	1.57(1)	N(2)–C(9)–C(10)	110.1(5)
C(18)–C(19)	1.50(1)	C(9)–C(10)–C(11)	112.3(5)
C(19)–C(20)	1.40(1)	C(10)–C(11)–C(12)	117.3(6)
C(20)–C(21)	1.37(1)	C(10)–C(11)–C(16)	121.4(6)
C(21)–C(22)	1.37(1)	C(11)–C(12)–C(13)	117.5(7)
C(22)–C(23)	1.40(1)	C(12)–C(13)–C(14)	121.9(8)
C(23)–C(24)	1.39(1)	C(13)–C(14)–C(15)	118.2(7)
C(24)–C(19)	1.38(1)	C(14)–C(15)–C(16)	121.6(7)
N(4)–C(25)	1.538(8)	C(15)–C(16)–C(11)	119.5(7)
C(25)–C(26)	1.47(1)	C(16)–C(11)–C(12)	121.2(6)
C(26)–C(27)	1.58(1)	N(3)–C(17)–C(18)	110.5(5)
C(27)–C(28)	1.39(1)	C(17)–C(18)–C(19)	114.7(5)
C(28)–C(29)	1.39(1)	C(18)–C(19)–C(20)	120.4(7)
C(29)–C(30)	1.38(2)	C(18)–C(19)–C(24)	120.4(6)
C(30)–C(31)	1.44(2)	C(19)–C(20)–C(21)	119.8(8)
C(31)–C(32)	1.38(1)	C(20)–C(21)–C(22)	122.4(8)
C(32)–C(27)	1.38(1)	C(21)–C(22)–C(23)	117.3(8)
Cl(1)–Pb(1)–Cl(4)	179.08(4)	C(22)–C(23)–C(24)	121.6(8)
Cl(1)–Pb(1)–Cl(5)	97.18(4)	C(23)–C(24)–C(19)	119.5(7)
Cl(1)–Pb(1)–Cl(6)	90.47(4)	C(24)–C(19)–C(20)	119.2(7)
Cl(1)–Pb(1)–Cl(7)	90.14(4)	N(4)–C(25)–C(26)	109.9(6)
Cl(1)–Pb(1)–Cl(8)	96.74(4)	C(25)–C(26)–C(27)	116.0(5)
Cl(4)–Pb(1)–Cl(5)	83.11(4)	C(26)–C(27)–C(28)	120.7(6)
Cl(4)–Pb(1)–Cl(6)	89.17(4)	C(26)–C(27)–C(32)	118.1(7)
Cl(4)–Pb(1)–Cl(7)	89.00(4)	C(27)–C(28)–C(29)	121.0(7)
Cl(4)–Pb(1)–Cl(8)	84.12(4)	C(28)–C(29)–C(30)	117.8(8)
Cl(5)–Pb(1)–Cl(6)	171.01(4)	C(29)–C(30)–C(31)	121.6(7)
Cl(5)–Pb(1)–Cl(7)	87.88(4)	C(30)–C(31)–C(32)	118.4(7)
Cl(5)–Pb(1)–Cl(8)	91.46(4)	C(31)–C(32)–C(27)	119.7(8)
Cl(6)–Pb(1)–Cl(7)	87.37(4)	C(32)–C(27)–C(28)	121.2(7)

[a] $1 + x, y, z$; [b] $2 - x, 1 - y, -z$; [c] $2 - x, -y, -z$; [d] $-1 + x, y, z$.

substantially different from 180° (i.e., 151.37(5)°–153.28(5)°), indicating that adjacent octahedra are substantially rotated and tilted relative to each other. The local Pb coordination in the present $(C_6H_5C_2H_4NH_3)_2PbCl_4$ structure is similar to that previously observed in $(C_3H_7NH_3)_2PbCl_4$ (21) and $NH_3(CH_2)_4NH_3PbCl_4$ (22). In $NH_3(CH_2)_4NH_3PbCl_4$, for example, there is a single independent Pb atom in the unit cell, with Pb–Cl bond lengths between 2.813(6) and 2.927(6) Å (2.878 Å average) and with Cl–Pb–Cl bond angles which range from 82.9(2)° to 98.5(2)° (90° for ideal octahedral coordination) (22).

The unit cell for $(C_6H_5C_2H_4NH_3)_2PbCl_4$ is not isostructural with that reported for either monoclinic $(C_6H_5C_2H_4NH_3)_2PbI_4$ (8) or orthorhombic $(C_6H_5C_2H_4NH_3)_2CuCl_4$ (23). Each of the triclinic unit cell dimensions within the plane of the perovskite sheets ($a = 11.1463(3)$ Å and $b = 11.2181(3)$ Å) are approximately twice the simple cubic perovskite lattice parameter, a_p. (The cubic perovskite $CH_3NH_3PbCl_3$, for example, has $a_p = 5.657(2)$ Å (24)). A survey of the organic–inorganic perovskite structures (e.g., Table II in Ref. (10)) indicates that related layered perovskites more typically adopt a $\sqrt{2}a_p \times \sqrt{2}a_p$ superstructure. In $(C_3H_7NH_3)_2PbCl_4$, for example, which has the phenethylammonium cation of the title compound replaced by propylammonium, the orthorhombic lattice constants are $a = 7.815(1)$ Å, $b = 7.954(1)$ Å, and $c = 25.034(3)$ Å (21). In $(C_6H_5C_2H_4NH_3)_2CuCl_4$, where lead(II) has been replaced by copper(II), the orthorhombic lattice constants are $a = 7.328(1)$ Å, $b = 7.295(1)$ Å, and $c = 38.618(5)$ Å (23). In fact, the $2a_p \times 2a_p$ superstructure is uncommon among the known layered perovskites. One other example of this type of superstructure is found in $(C_6H_5CH_2NH_3)_2CuBr_4$, which exhibits the monoclinic ($A2/a$) lattice constants, $a = 10.558$ Å, $b = 10.486$ Å, $c = 63.473$ Å, and $\beta = 98.08°$ (25) (although the full crystal structure has not been reported).

A view perpendicular to the perovskite sheets in the $(C_6H_5C_2H_4NH_3)_2MCl_4$ (M = Cu and Pb) structures (Fig. 4) highlights some factors that give rise to the different superstructures. In $(C_6H_5C_2H_4NH_3)_2CuCl_4$, each phenethylammonium cation sits nominally in a square which is defined by four nearest neighbor Cu atoms and the Cu–Cl–Cu linkages between them. If the $CuCl_6$ octahedra were perfect and not tilted or rotated relative to each other, and neglecting the conformation and ordering of the organic cation, the unit cell dimensions within the perovskite sheet would be defined by this $a_p \times a_p$ square. In the actual structure, tilting of the octahedra apices away from the perovskite sheet perpendicular (more than rotations of the octahedra within the plane of the perovskite sheet), as well as ordering of the organic cations, gives rise to the observed $\sqrt{2}a_p \times \sqrt{2}a_p$ superstructure. In $(C_6H_5C_2H_4NH_3)_2PbCl_4$, the square defined by the four nearest neighbor Pb atoms and the associated Pb–Cl–Pb linkages is substantially

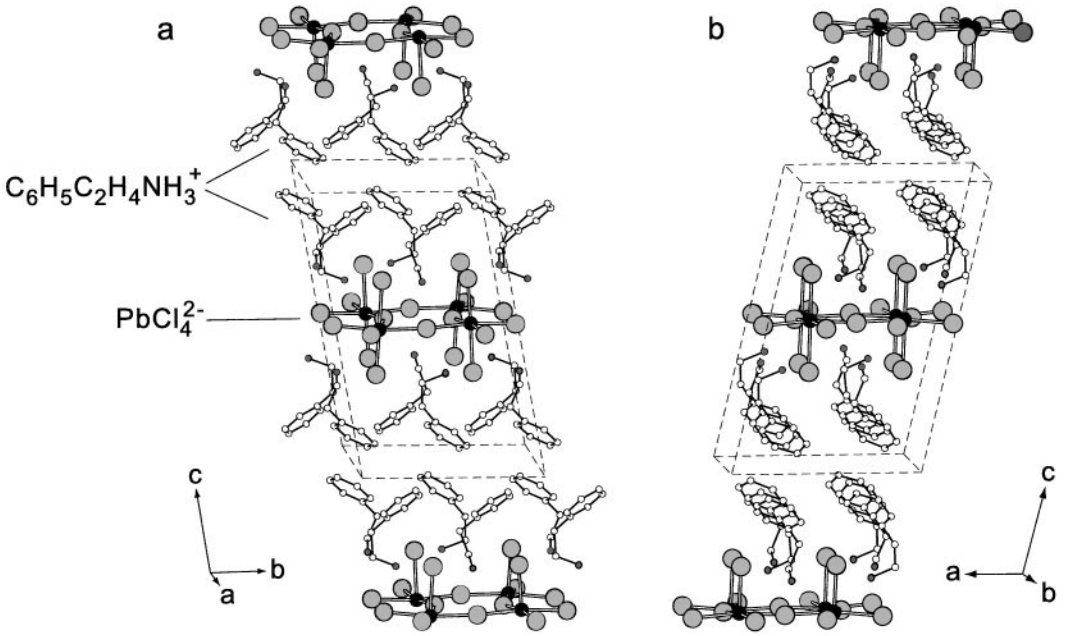

FIG. 3. Crystal structure of $(C_6H_5C_2H_4NH_3)_2PbCl_4$ viewed approximately down (a) the *a* axis and (b) the *b* axis. The unit cell outline is shown by the dashed lines. For clarity, the atoms are represented as spheres with uniform sizes selected for each atom type.

distorted by rotations of the $PbCl_6$ octahedra in the *a*–*b* plane. The $(C_6H_5C_2H_4NH_3)_2PbCl_4$ unit cell contains four independent phenethylammonium cations (labeled PE1–PE4 after the corresponding four nitrogen atoms). For the square at the center of the unit cell (around PE2), the square edges are pinched in along the *b* axis and pushed out along the *a* axis. The nearest neighbor squares along both the *a* and *b* directions (around PE3 and PE4) each have the opposite distortion (i.e., they are pinched in along the *a* axis and pushed out along the *b* axis). The repeat distance of this alternating distortion along each axis is two squares, thereby providing for the $2a_p \times 2a_p$ superstructure. The substantial difference between the ordering of the phenethylammonium cations in the $M = Cu$ and Pb structures highlights the important templating influence provided for the organic cations by the perovskite sheet. In turn, hydrogen bonding interactions with the phenethylammonium cation also play an important role in determining the distortions within the inorganic layers.

The four independent phenethylammonium cations within the $(C_6H_5C_2H_4NH_3)_2PbCl_4$ unit cell each have similar bond lengths and bond angles (Table 4) and these local parameters are similar to those observed for the same cation in $C_6H_5C_2H_4NH_2 \cdot HCl$ (26) and $(C_6H_5C_2H_4NH_3)_2CuX_4$ ($X = Cl$ and Br) (23). There is no evidence—either from unusual bond lengths, anomalous thermal parameters, or from extra peaks near the carbons in the final Fourier difference maps—of substantial disorder within the organic layer of the structure. As for the $C_6H_5C_2H_4NH_2 \cdot HCl$ and $(C_6H_5C_2H_4NH_3)_2CuX_4$ ($X = Cl$ and Br) structures (23, 26), the phenethylammonium thermal parameters in the title compound are consistently smallest for the ammonium group nitrogens ($3.4 < B_{iso}(N) < 4.3$ Å^2), which are hydrogen/ionic bonded to the halogens in the perovskite sheets. The largest parameters are found for the phenyl ring carbons, expecially those that are farthest from the ethylammonium cation fragment [$B_{iso}(C) > 6.0$ Å^2]. The slightly larger thermal parameters for the carbons farthest from the point of hydrogen bonding are expected since the bonding between adjacent layers of phenethylammonium cations is through relatively weak interactions between the phenyl rings. The weak interaction between layers enables more thermal motion at the far end of the molecule than at the end which is more firmly hydrogen bonded.

Closer examination of the four phenethylammonium cations reveals that they fall into two closely related conformational groups (Fig. 5). For both groups, all of the carbons in the phenyl ring, along with the first ethylammonium carbon attached to the ring, essentially lie in a plane. However, the terminal ethylammonium carbon and nitrogen atoms are not in the same plane and in fact, when viewed from the side (i.e., parallel to the plane of the phenyl group), the phenethylammonium molecules adopt a J-shaped conformation. The two groups can be distinguished by examining the positions of the terminal carbon and nitrogen atoms relative to the perpendicular bisecting plane of the phenyl group (In PE1, for example, the bisecting plane is perpendicular to the plane defined by the phenyl ring and intersects

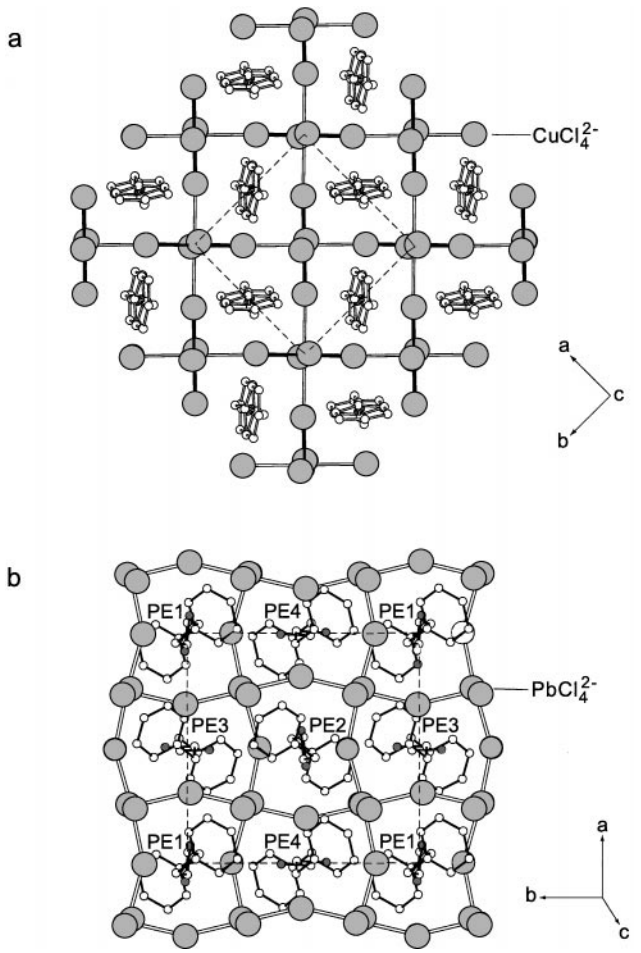

FIG. 4. A single layer of the $(C_6H_5C_2H_4NH_3)_2MCl_4$ structures, viewed perpendicular to the perovskite sheet for (a) $M = Cu$ and (b) $M = Pb$. The dashed lines indicate where the unit cell intersects with each perovskite layer, with the axes of the $M = Cu$ structure rotated by 45° with respect to those of the $M = Pb$ structure to achieve the same orientation relative to an ideal perovskite sheet. For the $M = Cu$ structure, the filled (or black) bonds represent short Cu–Cl bonds, while the open (or white) bonds represent elongated Cu ··· Cl semicoordinate bonds, resulting from the Jahn–Teller distortion of the $CuCl_6$ octahedra. Atomic coordinates for the $M = Cu$ compound are adopted from Willett (23). For clarity, all atoms are represented as spheres, with an arbitrary size selected for each atom type.

the C3 and C6 atoms). Viewed from the front, the ethylammonium fragment curves to the right of the plane in the first group (PE1 and PE3) and to the left in the second group (PE2 and PE4). Consequently, these conformers can be referred to as "right-handed" and "left-handed." The phenethylammonium cations on the top and bottom halves of the unit cell (along the *c*-axis) are related by inversion. Each Phenethylammonium cation switches groups under inversion—i.e., whereas on the top half, PE1 and PE3 are right-handed, on the bottom half they are left-handed (and vice versa for PE2 and PE4). Within a given layer of organic cations, the two groups are arranged by alternating rows of PE1/PE3 and PE2/PE4 cations, with the rows extending along the *a* axis of the structure (Fig. 4).

Note that the phenethylammonium cations in $C_6H_5C_2H_4NH_2 \cdot HCl$ (26) and $(C_6H_5C_2H_4NH_3)_2CuX_4$ (X = Cl or Br) (23) adopt a different conformation (Fig. 5). In both of these cases, there is a single independent phenethylammonium cation in the unit cell and the ethylammonium fragment curves downward, rather than to the right or left. The resulting *trans* conformation for the ethylammonium fragment (N(1)–C(1)–C(2)–C(3)) is expected to be the most stable configuration for the free molecule (11). Apparently, in the lead(II) chloride-based perovskite, the specific hydrogen bonding interactions and the constraints imposed by the distorted perovskite framework stabilize the unusual J-shaped phenethylammonium conformation.

As a result of the geometric constraints of the ammonium group and the organic tail in organic–inorganic layered perovskite structures, the primary N–H ··· X (X = Cl, Br, or I) hydrogen bonding interactions are expected to be either with two terminal and one bridging halogen (terminal halogen configuration) or with two bridging and one terminal halogen (bridging halogen configuration) (10, 27). The terminal halogen configuration is often adopted by systems with more bulky organic cations since this geometry reduces the interaction between the organic molecule and the terminal halogens. The $(C_6H_5C_2H_4NH_3)_2CuX_4$ (X = Cl and Br) structures, however, adopt the bridging halogen hydrogen bonding configuration, with N ··· Cl distances between the ammonium nitrogen and the nearest three chlorides ranging between 3.27–3.37 Å (23). In these structures, the antiferrodistortive arrangement of the long semi-coordinate Cu–X bonds in the plane of the perovskite sheets (resulting from the Jahn–Teller distortion of the CuX_6 octahedra) enables a strong interaction between the ammonium tail of the phenethylammonium cation and the two bridging halogens, without the phenethyl fragment interfering with the terminal halogens.

In the analogous lead(II) chloride structure, there is less flexibility within the inorganic framework. The hydrogens of the phenethylammonium cation in this structure have been located (Fig. 6) using the final difference Fourier map (although the unconstrained refinement of these atoms is unstable), demonstrating that each phenethylammonium cation adopts the terminal halogen configuration. The hydrogens of N(1) (N(2)) interact most strongly with terminal Cl(1) and Cl(3) (Cl(2) and Cl(4)) and bridging Cl(6) (Cl(5)) chlorides, while the hydrogens of N(3) (N(4)) interact primarily with terminal Cl(3) and Cl(4) (Cl(3) and Cl(4)) and bridging Cl(7) (Cl(8)) chlorides. Note that while the terminal chloride hydrogen bonding interactions involve a single chloride ion for each hydrogen (i.e., there is an ~1 Å difference between the primary H ··· Cl distance and the next

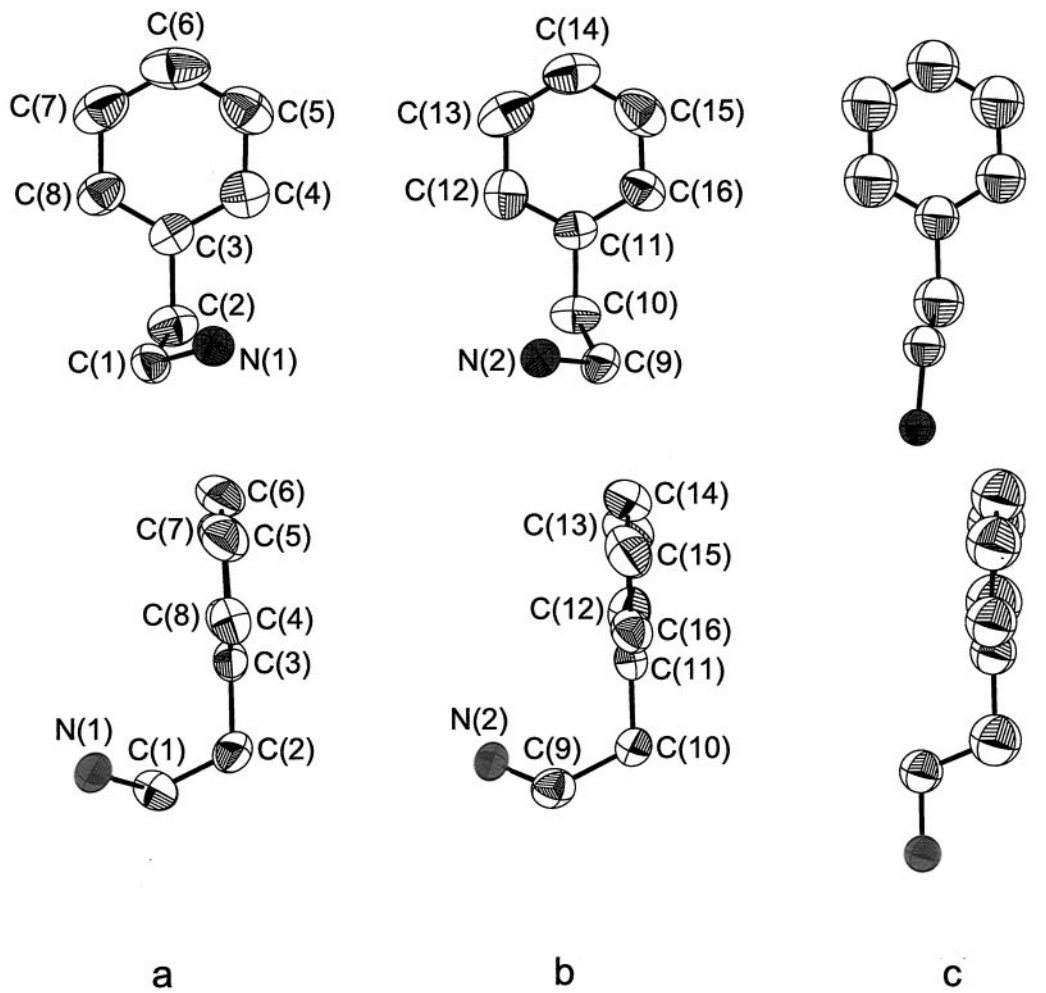

FIG. 5. Two related conformations for the phenethylammonium cations (a) PE1/PE3 and (b) PE2/PE4 from the top half of the $(C_6H_5C_2H_4NH_3)_2PbCl_4$ unit cell. The thermal ellipsoids are drawn at 50% probability. In (c), the conformation of the phenethylammonium cation in $(C_6H_5C_2H_4NH_3)_2CuCl_4$ is shown (23). Upper panels represent the front view, and lower panels represent the side view of each cation.

closest interaction), the interaction involving the bridging chlorides is somewhat less clear-cut. For the PE1 ammonium group, for example, while the primary interaction for the down-pointing (into the perovskite sheet) hydrogen is with one Cl(6) chloride, there are also similar distance (within $\sim$0.4 Å) interactions with other bridging chlorides.

The N $\cdots$ Cl distances between N(1) and N(2) and the closest three chloride atoms for each nitrogen are similar and range from 3.203(4) to 3.277(5) Å, while those for N(3) and N(4) range from 3.302(5) Å to 3.349(5) Å, reflecting a difference in hydrogen bonding for the two groups. This difference may account for the deduction from ^{1}H NMR data that there should be two distinguishable and equally populated types of NH_3 sites in the $(C_6H_5C_2H_4NH_3)_2PbCl_4$ structure (11). For PE1 and PE2, the plane containing the three ammonium group hydrogens is parallel to the *b* axis (Fig. 6) and the tilting/rotations of the $PbCl_6$ octahedra result in a stabilization of the hydrogen bonds (i.e., they tilt and rotate such that the bridging and terminal chlorides move closer to the ammonium group). For N(3) and N(4), the plane of the hydrogens is parallel to the *a* axis. The tilting and distortion of the octahedra is such that the terminal chlorides, Cl(3) and Cl(4), are slightly further from the corresponding nitrogen atoms compared to the terminal chlorides for PE1 and PE2. Consequently, within an organic cation layer, each pair of cations with the same conformation (PE1/PE3 and PE2/PE4) can further be distinguished by the two orientations of hydrogen bonding. Note that the alternation in the direction of the plane containing the ammonium group hydrogens corresponds to the alternation in the distortions in the perovskite sheet (described above).

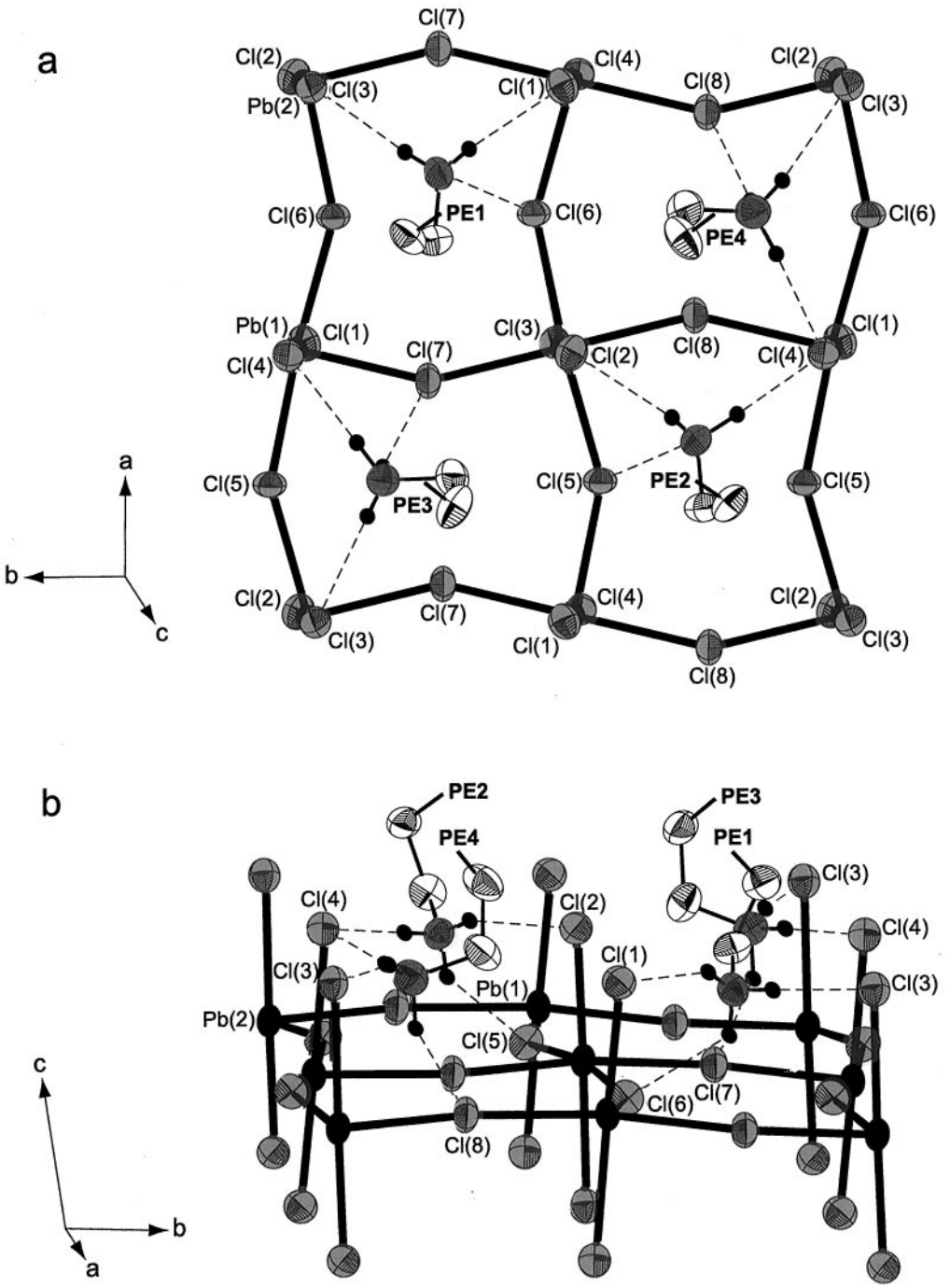

FIG. 6. Primary hydrogen bonding interactions (dashed line) between the ammonium head of each phenethylammonium cation and the halogens in the perovskite sheets. The two views of the structure are approximately along (a) the *c* axis and (b) the *a* axis, with the thermal ellipsoids for the nonhydrogen atoms drawn at 50% probability. The unrefined positions of the hydrogen atoms have been determined from the final Fourier difference map and these atoms are drawn as spheres with arbitrary size. For clarity, only the ethylammonium fragment of each phenethylammonium cation and the ammonium group hydrogens are shown.

CONCLUSIONS

Often, one of the key limiting factors in crystallographic studies is the quality of the crystals available. This is especially true for many of the layered organic–inorganic perovskites (10), where the crystals tend to grow as thin sheets. In this contribution, a layered solution technique has been described, which is similar in concept to the gel technique

except that the slow diffusion between the components is controlled by the density difference and degree of miscibility of multiple solution layers. Thick crystals of $(C_6H_5C_2H_4NH_3)_2PbCl_4$ have been grown using the layered solution technique, enabling a careful examination of the crystal structure of this compound.

The ordered crystal structure found here for $(C_6H_5C_2H_4NH_3)_2PbCl_4$ is distinct from the disordered model reported (8) for $(C_6H_5C_2H_4NH_3)_2PbI_4$, as well as from the fully ordered cell for $(C_6H_5C_2H_4NH_3)_2CuCl_4$ (23). Whereas the ordered copper(II) analog adopts a more typical layered perovskite framework with a $\sqrt{2}a_p \times \sqrt{2}a_p$ superstructure in the plane of the perovskite sheets, the lead(II) chloride compound presents a $2a_p \times 2a_p$ superstructure. This superstructure arises from rotation/tilting of the $PbCl_6$ octahedra of the perovskite sheet, as well as from organic cation ordering, and is expected to be observed in other layered perovskite frameworks—especially those with more complex (or bulky) organic cations. In contrast to the $(C_6H_5C_2H_4NH_3)_2CuX_4$ (X = Cl and Br) structures, where the organic cation interacts with the perovskite sheets using a bridging halogen configuration and the phenethylammonium cation ethylammonium group adopts a *trans* conformation, in $(C_6H_5C_2H_4NH_3)_2PbCl_4$, the phenethylammonium cation hydrogen bonds using a terminal halogen hydrogen bonding scheme and adopts a less favorable J-shaped conformation. This difference apparently arises because of structural and electronic differences between the metal halide frameworks (e.g., presence or absence of a Jahn–Teller distortion).

In addition to the $(C_6H_5C_2H_4NH_3)_2PbCl_4$ structure, powder X-ray diffraction data (5) for the series, $(C_6H_5C_2H_4NH_3)_2PbCl_xBr_{4-x}$, has previously demonstrated a smooth progression in the c-axis dimension as a function of x, suggesting that the two endpoints might be isostructural. In fact, a preliminary study of the $(C_6H_5C_2H_4NH_3)_2PbBr_4$ structure, using a crystal grown by the layered solution approach, indicates that a stable but only marginally satisfactory refinement can be achieved using the same cell as for the chloride. The cell and preliminary refinement parameters for this model are $a = 11.6070(5)$ Å, $b = 11.6236(5)$ Å, $c = 17.5935(8)$ Å, $\alpha = 99.521(1)^\circ$, $\beta = 105.710(1)^\circ$, $\gamma = 89.996(1)^\circ$, $V = 2251.0(2)$ Å^3, $R_f/R_w = 11.49/12.95$. A substantial number of unindexed reflections in the initial indexing of the cell, which correspond to a doubling or quadrupling of the c axis, and relatively large residual peaks in the final Fourier difference map, each suggest that while the bromide and chloride structures are very similar, they may not be isostructural (i.e., there is perhaps a further superstructure in the lead(II) bromide compound). A more complete analysis of the $(C_6H_5C_2H_4NH_3)_2PbBr_4$ structure is currently underway.

ACKNOWLEDGMENT

The authors gratefully acknowledge DARPA for partial support of this work under Contract DAAL01-96-C-0095.

REFERENCES

1. X. Hong, T. Ishihara, and A. V. Nurmikko, *Phys. Rev. B* **45,** 6961 (1992).
2. G. C. Papavassiliou and I. B. Koutselas, *Synth. Metals* **71,** 1713 (1995).
3. N. Kitazawa, *Jpn. J. Appl. Phys.* **35,** 6202 (1996).
4. N. Kitazawa, *Jpn. J. Appl. Phys.* **36,** 2272 (1997).
5. N. Kitazawa, *Mater. Sci. Engng. B* **49,** 233 (1997).
6. X. Hong, T. Ishihara, and A. V. Nurmikko, *Solid State Commun.* **84,** 657 (1992).
7. M. Era, S. Morimoto, T. Tsutsui, and S. Saito, *Appl. Phys. Lett.* **65,** 676 (1994).
8. J. Calabrese, N. L. Jones, R. L. Harlow, N. Herron, D. L. Thorn, and Y. Wang, *J. Am. Chem. Soc.* **113,** 2328 (1991).
9. T. Fujita, Y. Sato, T. Kuitani, and T. Ishihara, *Phys. Rev. B* **57,** 12428 (1998).
10. For a recent review see D. B. Mitzi, *Prog. Inorg. Chem.* **48,** 1 (1999).
11. T. Ueda, M. Oma, K. Shimizu, H. Ohki, and T. Okuda, *Z. Naturforsch.* **52a,** 502 (1997).
12. G. M. Sheldrick, "SADABS." Institut für Anorganische Chemie der Universität Göttingen, 1997.
13. E. J. Gabe, Y. Le Page, J.-P. Charland, F. L. Lee, and P. S. White, *J. Appl. Crystallogr.* **22,** 384 (1989).
14. Y. Le Page, *J. Appl. Crystallogr.* **21,** 983 (1988).
15. H. Arend, W. Huber, F. H. Mischgofsky, and G. K. Richter-Van Leeuwen, *J. Cryst. Growth* **43,** 213 (1978).
16. D. B. Mitzi, *Chem. Mater.* **8,** 791 (1996).
17. T. Ishihara, J. Takahashi, and T. Goto, *Phys. Rev. B* **42,** 11099 (1990).
18. S. L. Suib and P. F. Weller, *J. Cryst. Growth* **48,** 155 (1980).
19. T. Ishihara, *in* "Optical Properties of Low-Dimensional Materials" (T. Ogawa and Y. Kanemitsu, Eds.), p. 288. World Scientific, Singapore 1995.
20. S. Wang, D. B. Mitzi, P. Meng, and J. Moore, unpublished results.
21. A. Meresse and A. Daoud, *Acta Crystallogr. C* **45,** 194 (1989).
22. C. Courseille, N. B. Chanh, Th. Maris, A. Daoud, Y. Abid, and M. Leguerre, *Phys. Stat. Sol.* (*a*) **143,** 203 (1994).
23. R. D. Willett, *Acta Crystallogr. C* **46,** 565 (1990).
24. O. Knop, R. E. Wasylishen, M. A. White, T. S. Cameron, and M. J. M. Van Oort, *Can. J. Chem.* **68,** 412 (1990).
25. P. Zhou, J. E. Drumheller, B. Patyal, and R. D. Willett, *Phys. Rev. B* **45,** 12365 (1992).
26. P. G. Tsoucaris, *Acta Crystallogr.* **14,** 909 (1961); E. Horn, E. R. T. Tiekink, G. P. Jones, B. P. Naiola, and L. G. Paleg, *Acta Crystallogr. C* **46,** 1575 (1990).
27. G. Chapuis, R. Kind, and H. Arend, *Phys. Stat. Sol.* (*a*) **36,** 285 (1976).